

BiMn₇O₁₂: Polar antiferromagnetism by inverse exchange strictionDylan Behr,^{1,*} Alexei A. Belik,² Dmitry D. Khalyavin,³ and Roger D. Johnson¹¹*Department of Physics and Astronomy, University College London, Gower Street, London WC1E 6BT, United Kingdom*²*International Center for Materials Nanoarchitectonics (MANA), National Institute for Materials Science (NIMS), 1-1 Namiki, Tsukuba, Ibaraki 305-0044, Japan*³*ISIS facility, Rutherford Appleton Laboratory-STFC, Chilton, Didcot OX11 0QX, United Kingdom*

(Received 21 September 2022; accepted 1 February 2023; published 3 April 2023)

Despite extensive research on magnetically induced ferroelectricity there exist relatively few studies on how a preexisting electric polarization affects magnetic order. Given that well-established magnetoelectric coupling schemes can in principle work in reverse, one might anticipate that primary, polar magnetic structures could be uniquely stabilized in ferroelectric crystals, however, this scenario is apparently rare. Here, we show that in ferroelectric BiMn₇O₁₂, a pure, polar *E*-type antiferromagnetic order emerges below $T_1 = 59$ K, and we present a phenomenological model of trilinear magnetoelectric coupling consistent with Bi³⁺ lone-pair driven polar distortions uniquely stabilizing the polar antiferromagnetism via modulation of Heisenberg exchange pathways, i.e., inverse exchange striction. In addition, below $T_2 = 55$ K there occurs large commensurate canting of the *E*-type structure due to the onset of ferrimagnetic order on a separate crystallographic sublattice that may be exploited for additional magnetoelectric functionality.

DOI: [10.1103/PhysRevB.107.L140402](https://doi.org/10.1103/PhysRevB.107.L140402)

Multiferroic materials in which magnetic and ferroelectric (FE) orders coexist in a single phase have attracted considerable attention within condensed matter and materials physics due to their fascinating fundamental phenomenology and applicable functionalities should the two orders couple [1–3]. In type II multiferroics magnetic order appears concomitantly with FE polarization, implying magnetoelectric (ME) coupling in the form of a trilinear invariant that couples the polarization to two magnetic order parameters [4]. In the canonical type II multiferroic TbMnO₃, for example, incommensurate magnetic order stabilized by frustrated exchange undergoes a transition from a centrosymmetric collinear spin density wave to a noncollinear polar spin cycloid inducing a FE polarization via the inverse Dzyaloshinskii-Moriya (DM) mechanism [5–7].

The possibility of ME coupling by exchange striction between collinear spins has generated considerable excitement, owing to the promise of stronger coupling from Heisenberg interactions compared to the weak, spin-orbit based DM interaction. For example, in the type II multiferroic Ca₃CoMnO₆ frustrated Heisenberg exchange produces $\uparrow\uparrow\downarrow\downarrow$ magnetic order on one-dimensional (1D) Ising chains [8]. This order breaks inversion symmetry and generates a polarization, which, to good approximation, is proportional to the spatial derivative of the Heisenberg exchange along the direction of the magnetic propagation vector [9]. This mechanism could also explain type II multiferroicity in the orthorhombic *o*-RMnO₃ manganites ($R = \text{Ho, Tm, Yb, Lu}$). In these systems a two-dimensional manifestation of the $\uparrow\uparrow\downarrow\downarrow$ -type order is realized in the form of a polar *E*-type antiferromagnetic

(AFM) structure [10–12]. The coherent modulation of exchange induces distortions in bond angles and local electron densities, which together create a net electric polarization [13,14].

Type I multiferroics exhibit FE order at temperatures above spontaneous magnetic ordering. In this case direct coupling between the two is neither implied nor common; in most cases the magnetic structure arises independently of ferroelectricity, can be described to good approximation in the centrosymmetric limit, and the two orders are essentially decoupled [15,16]. In some cases ME coupling can emerge but not as an intrinsic phenomenon. For example, the hexagonal rare earth manganites (*h*-RMnO₃) display ME coupling via a complex mechanism involving topological defects at the domain walls [16,17]. Arguably the best studied type I multiferroic with intrinsic ME coupling is BiFeO₃, in which Lifshitz invariants in the free energy [18,19] allowed by polar distortions map onto direct DM interactions. These induce a long-period cycloidal modulation of an otherwise centrosymmetric collinear *G*-type antiferromagnet [20,21]. Still, the effect of polarization on the magnetic structure might be considered perturbative as a given unit cell has an approximately centrosymmetric collinear magnetic structure, and pure *G*-type phases can be readily stabilized by small levels of chemical substitution despite the large FE polarization [22,23]. Aside from BiFeO₃, there exist few examples of “polar” magnetic structures uniquely stabilized in the presence of ferroelectricity. One other example is metallic bilayer ruthenate Ca₃Ru₂O₇ where a spin cycloid is again stabilized by DM interactions in the proximity of collinear spin reorientation [24]. Beyond the above DM-based coupling schemes, systems hosting inverse exchange striction ME coupling are lacking.

In this Letter we show that the proper FE quadruple perovskite BiMn₇O₁₂ (general formula AA′B₄O₁₂) fulfills

*dylan.behr.20@ucl.ac.uk

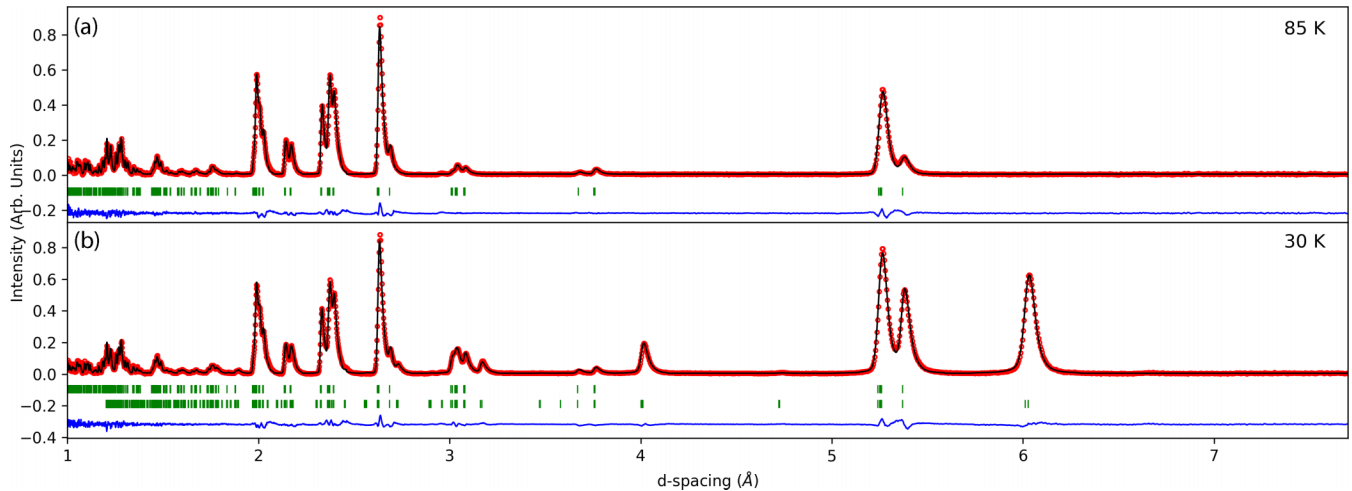


FIG. 1. Neutron powder diffraction data (red circles) measured in (a) the paramagnetic phase above T_1 and (b) between T_2 and T_3 . Fits to the data are shown as solid black lines, the differences between data and fit are shown as solid blue lines below, and the position of nuclear and magnetic Bragg peaks indexing at $\mathbf{k}_2 = (0, 0, 0)$, and magnetic Bragg peaks indexing at $\mathbf{k}_1 = (\frac{1}{2}, 0, -\frac{1}{2})$ are marked by top and bottom green tick marks, respectively.

the above criteria. We present a symmetry-based approach demonstrating that a pure E -type AFM phase at $T_1 = 59$ K is stabilized by a ME trilinear invariant, here related to nearest-neighbor Heisenberg exchange modulated by the FE distortions. We further resolve C -type ferrimagnetic (FIM) and AFM modes on the Mn A' and B sites, respectively, that onset on further cooling below $T_2 = 55$ K. The bulk magnetization provided by this secondary phase, not exhibited in BiFeO_3 or $h\text{-RMnO}_3$ systems, offers an avenue towards additional ME properties.

A polycrystalline sample of $\text{BiMn}_7\text{O}_{12}$ in the form of a fine powder was synthesized under high-pressure, high-temperature conditions from stoichiometric mixtures of Bi_2O_3 and Mn_2O_3 starting reagents as detailed in Ref. [25]. Neutron powder diffraction experiments were performed using the time-of-flight diffractometer WISH at ISIS [26]. A 785-mg sample was loaded into a cylindrical 3-mm-diameter vanadium can and cooled to a base temperature of 1.5 K. Diffraction data with good counting statistics were collected on warming from 5 to 85 K in 5-K steps, 50 to 64 K in 1-K steps, and additionally, data with high counting statistics were collected at 85, 30 and 1.5 K. Rietveld refinements of the crystal and magnetic structures were performed using FULLPROF [27] while symmetry analyses employed the ISOTROPY software suite [28,29]. Magnetic susceptibility measurements were performed on a Quantum Design magnetic property measurement system (MPMS-3) between 2 and 350 K in a 100 Oe field under both zero-field-cooled (ZFC) and field-cooled-on-cooling (FCC) conditions. Isothermal magnetization measurements were performed between -70 and 70 kOe at 2 and 40 K. Heat capacity measurements were made in 0 and 90 kOe fields using a Quantum Design physical property measurement system (PPMS).

$\text{BiMn}_7\text{O}_{12}$ undergoes a complex sequence of structural phase transitions at 608, 460, and 290 K: from the $\text{RMn}_7\text{O}_{12}$ aristotype $Im\bar{3}$ at high temperature, through $I2/m$, Im [30], and finally $P1$ in the ground state [31] [we will use an I -centered unit cell ($I1$) to describe the low-temperature crystal

structure in the same basis as the higher-symmetry phases]. These transitions were characterized by the onset of orbital order, FE polarization in the mirror plane perpendicular to \mathbf{b} , and the polarization lifting out of the ac plane, respectively [25]. A Rietveld-refined $I1$ structural model gives good agreement to nuclear intensities observed in our neutron powder diffraction (NPD) data measured at 85 K [see Fig. 1(a) and Table S1 in the Supplemental Material [32]].

$\text{BiMn}_7\text{O}_{12}$ was reported to have two magnetic phase transitions at temperatures $T_{N,B} = 55$ K and $T_{N,A'} = 25$ K [33,34]. It was shown in this previous study that below $T_{N,B}$, B sites developed canted AFM order with zero net moment and described by two propagation vectors, $\mathbf{k}_1 = (\frac{1}{2}, 0, -\frac{1}{2})$ [35] and $\mathbf{k}_2 = (0, 0, 0)$. To the contrary, the specific heat data shown in Fig. 2(a) resolve not just one but two transitions on cooling through $T_{N,B}$, which we label T_1 and T_2 , respectively. The detection of a possible further phase transition in the vicinity of $T_{N,B}$ was first reported by Imamura *et al.* [36] but its origin was not resolved. The magnetic susceptibility [Fig. 2(b)] showed no detectable anomaly at T_1 , while a sizable net magnetization appeared below T_2 consistent with the onset of FIM order [see also M vs H hysteresis in the bottom-left inset to Fig. 2(b)]. NPD measurements over the range 50–64 K revealed the thermal separation of two distinct sets of magnetic Bragg peaks at T_1 and T_2 , indexing with propagation vectors \mathbf{k}_1 and \mathbf{k}_2 , respectively (see Fig. 3), that is, there exists a pure \mathbf{k}_1 phase for $T_2 < T < T_1$, and a mixed $\mathbf{k}_1 + \mathbf{k}_2$ phase for $T < T_2$. This observation reconciles the apparent absence of a first-order phase transition at $T_{N,B}$, which would be implied by the simultaneous onset of two orders with different propagation vectors. Indeed, a first-order transition would have been evidenced in heat capacity as thermal hysteresis across a single magnetic transition at this temperature, which is not seen in our bulk measurements. Below $T_{N,A'}$, A' sites were found to adopt AFM order with a propagation vector $\mathbf{k}_2 = (0, 0, 0)$. We note that $T_{N,A}$ was observed in our sample and labeled T_3 in Fig. 2.

The previously reported \mathbf{k}_1 component corresponding to an E -type AFM order on the B sublattice [33] was refined

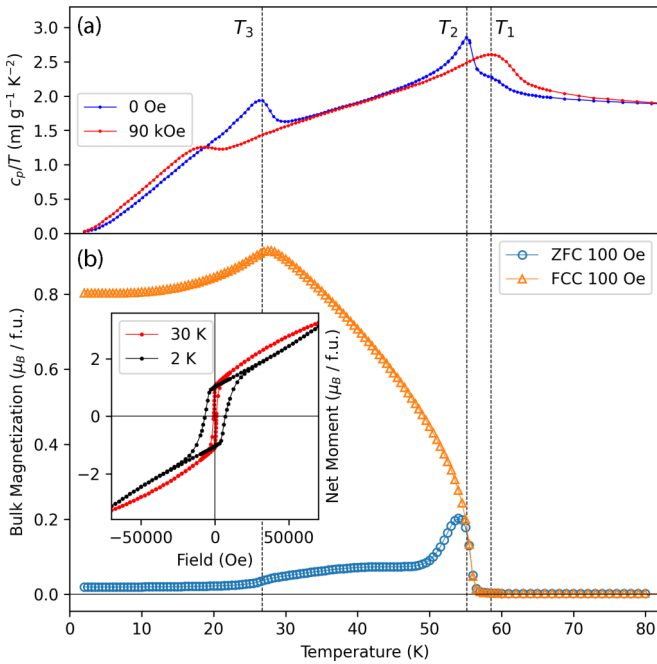


FIG. 2. (a) Specific heat capacity over temperature of BiMn₇O₁₂ in zero applied field and 90 kOe. The data plotted were collected on cooling, but heating and cooling curves had no substantial differences. Magnetic transitions inferred from anomalous features in the heat capacity and are indicated by vertical dashed lines. (b) ZFC and FCC magnetization measurements of polycrystalline BiMn₇O₁₂ under an applied dc field of 100 Oe. The inset shows isothermal moment vs field measurements at temperatures 2 and 30 K.

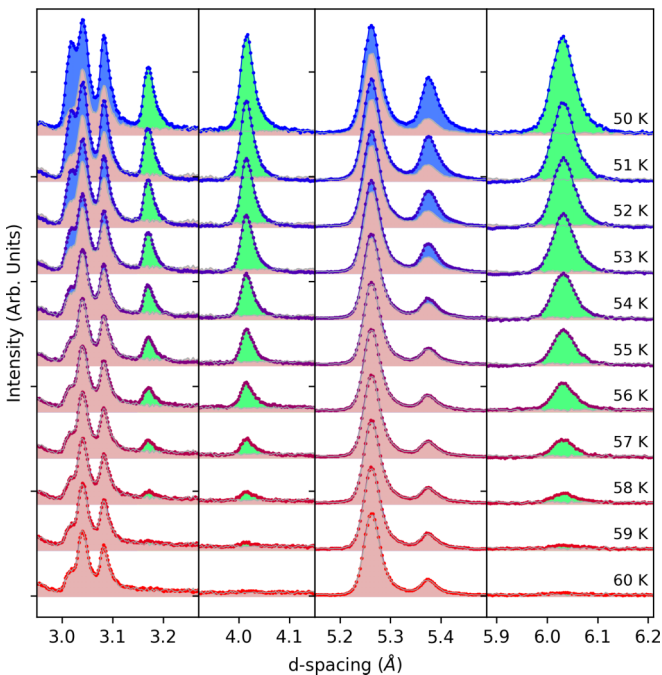


FIG. 3. Evolution of selected NPD intensities through magnetic transitions at $T_1 = 59$ K and $T_2 = 55$ K. Nuclear intensities from data collected at 64 K in the paramagnetic phase are shaded in red, while magnetic intensities indexing at $\mathbf{k}_1 = (\frac{1}{2}, 0, -\frac{1}{2})$ and $\mathbf{k}_2 = (0, 0, 0)$ are indicated in green and blue, respectively. Intensities of selected d-spacing ranges have been nonuniformly rescaled for clarity.

against NPD data measured at 30 K, here constrained to the true $I1$ parent symmetry. We found excellent agreement ($R_{\text{Mag}} = 4.18\%$), and the results are shown in Fig. 4(a) and Table S1 [32]. We note that while the 30 K phase has an admixture of \mathbf{k}_1 and \mathbf{k}_2 magnetic orders, the respective Bragg peaks are well separated and the larger magnetic intensity at low temperature allowed for a more precise refinement. The intensities of the \mathbf{k}_1 peaks, relative to each other, did not vary with temperature. Hence this refinement is representative of the \mathbf{k}_1 structure at all temperatures, up to a global moment magnitude.

In the refinement of the \mathbf{k}_2 component developing below T_2 we considered magnetic order on both A' and B sublattices. Systematic tests led us to conclude that A' sites adopt FIM order simultaneously with large B site AFM canting, immediately below T_2 (see Fig. 4 and Table S1 [32]). Crucially, this FIM \mathbf{k}_2 structure at the A' sites accounts for the significant uncompensated moment observed in magnetometry [see Fig. 2(b) inset], with good agreement between the refined FIM moment size and that inferred from the powder-averaged remnant magnetization at 30 K ($2.2\mu_B/\text{f.u.}$ vs $2.1\mu_B/\text{f.u.}$, respectively). In previous reports the net moment has been attributed to DM-induced FM spin canting [30,34,36], but this would normally be considered too weak to produce such large magnetization. Furthermore, the magnetic structure reported by Gauzzi *et al.* [33], being fully AFM, failed to account for a net moment below $T_{N,B}$. The present description of the magnetic transitions also accords well with specific heat measurements in an applied field of 90 kOe [Fig. 2(a)], where the apparent field-induced shift in T_2 up to a temperature indistinguishable from T_1 can be explained by Zeeman coupling to the FIM moment. The B site canting is characterized by an additional superposed C -type mode, with the B site moments canting in the direction of the A' site moments, perpendicular to the preexisting E -type AFM order [see Fig. 4(b)]. We note that this B site magnetic structure below T_2 is similar to that previously reported below $T_{N,B}$ [33], except that the \mathbf{k}_2 component lies in the ac plane rather than along \mathbf{b} . Altogether, a more than fourfold reduction in χ^2 is achieved when refining the above dual sublattice model ($\chi^2 = 6.8$) instead of the single sublattice solution of Ref. [33] ($\chi^2 = 29.8$). Furthermore, the refined \mathbf{k}_2 magnetic order closely resembles the FIM and AFM structures found on the A' and B sites in all other $I2/m$ RMn₇O₁₂ ($R = \text{rare earth or Y}$) compounds studied to date [37]. These observations indicate that the \mathbf{k}_2 order is ubiquitous to the extended $A^{3+}\text{Mn}_7\text{O}_{12}$ family with a common physical origin, while the E -type order is unique to the Bi³⁺ compound.

Below $T_3 = 27$ K a third set of magnetic Bragg peaks appear in NPD data that index with a propagation vector $\mathbf{k}_3 = (0, 1, 0)$, consistent with previous reports [33]. This propagation vector implies the admixture of additional AFM modes, consistent with the reduction in net FIM moment observed in magnetometry data [Fig. 2(b)], and the suppression of T_3 at high fields [Fig. 2(a)]. We suggest that this transition warrants further investigation given the magnetic structure solutions described above, but this falls outside the scope of the present work.

Taking the $I2/m$ crystal structure as a higher-symmetry, centrosymmetric parent (found for $460 < T < 608$ K), one

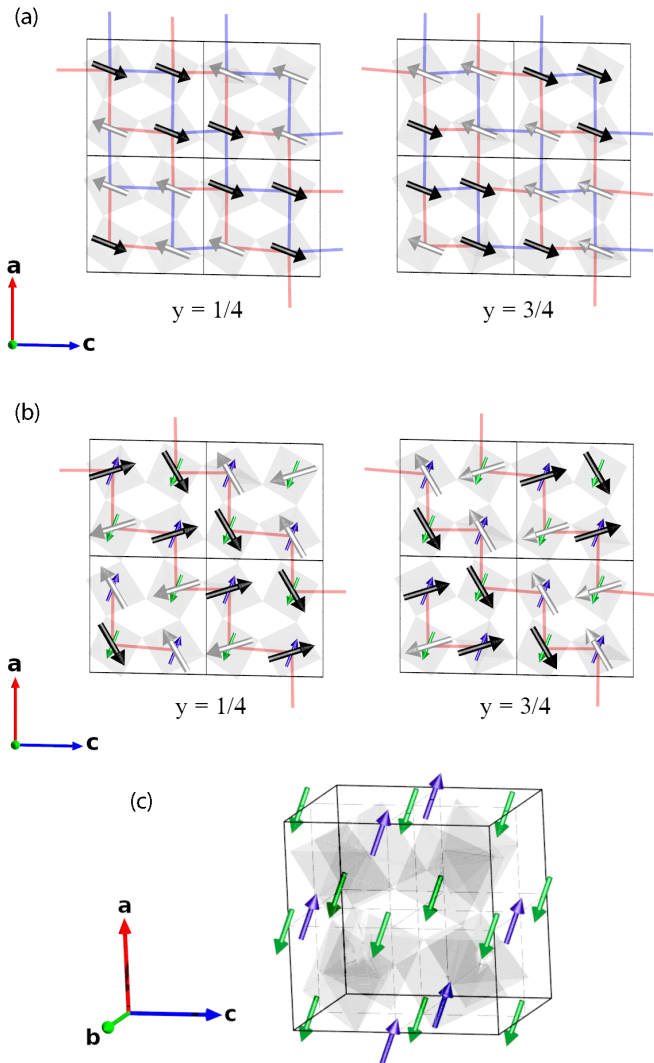


FIG. 4. Magnetic unit cells of $\text{BiMn}_7\text{O}_{12}$ at 30 K. (a) E -type component of magnetic structure in approximate ac -planar layers of B sites in the lower (left) and upper (right) halves of the unit cell along b . The order forms FM (AFM) zigzag chains indicated in blue (red) running along $a - c$. Paramagnetic unit cell boundaries are indicated by straight black lines. (b) Orthogonal C -type modes (blue and green arrows) result in a canting of the preexisting E -type structure. (c) FIM structure on A' sites in a single paramagnetic unit cell, arising concomitantly with a C -type component on B sites.

can show that the polar E -type magnetic structure decomposes into two separate magnetic modes to which we assign order parameters η_1 and η_2 that transform by different irreducible representations (irreps), mA_1^+ and mA_2^- , respectively. The mode transforming by mA_1^+ includes B site moments only at the $4e$ Wyckoff position of the $I2/m$ unit cell, while that transforming by mA_2^- has moments only at the $4f$ position (see Table S4 of the Supplemental Material [32]). In this symmetry there exists no bilinear coupling of the form $\eta_1\eta_2$, hence nearest-neighbor interactions between the two modes exactly cancel by symmetry and the E -type structure is not stable. In contrast, taking either polar Im or $I1$ crystal structures as the parent reveals that the full E -type structure

transforms by a single magnetic irrep (mA_1), with nearest-neighbor magnetic coupling allowed by symmetry between all B sites. This points to the significance of the polar distortion in stabilizing the polar magnetic structure. Returning to the $I2/m$ parent, one can show that the FE distortions that lower the crystal symmetry to Im transform by the irrep Γ_2^- with order parameter δ (see Table S4 [32]). A systematic analysis of symmetry-allowed free-energy invariants using ISOTROPY [28] demonstrates the existence of a trilinear invariant of the form $\delta\eta_1\eta_2$, which stabilizes E -type magnetic order on the B sites via the polar distortions (N.B. this invariant involves only E -type components with moments in the ac plane, as observed in the NPD refinement).

The large $a^+a^+a^+$ -type octahedral rotations that characterize the quadruple perovskite's aristotype $Im\bar{3}$ structure give rise to Mn-O-Mn bond angles of around 135° . In this case B - B exchange interactions are delicately poised between FM and AFM, owing to numerous competing exchange pathways across a single Mn-O-Mn bond. The modulation imposed by the polar distortion includes large displacements of oxygen ions that mediate the B - B exchange. The pattern of displacements (Γ_2^- symmetry) can then in principle select an alternating sequence of FM and AFM exchange interactions that stabilize the observed B site E -type magnetic structure below T_1 [Fig. 4(a)]. This mechanism is in direct analogy with that describing the ME coupling in type II multiferroic α - RMnO_3 systems [10,14], and can be considered a prototypical example of ME coupling in a type I multiferroic based on inverse exchange striction.

While the B - B exchange is solely responsible for the E -type structure observed between T_1 and T_2 , the additional \mathbf{k}_2 modes appearing below T_2 are likely stabilized by A - B interactions, as proposed for the wider $\text{RMn}_7\text{O}_{12}$ family [37]. In this case $\text{BiMn}_7\text{O}_{12}$ would host a 3D network of frustrated nearest-neighbor A - B and next-nearest-neighbor B - B interactions that are accommodated by the spin canting. Although the FIM and C -type canting modes do not directly couple to the FE polarization, the net moment associated with the FIM component on A' sites may still offer ME functionality. In CoCr_2O_4 , for instance, despite direct coupling of \mathbf{P} only to the AFM in-plane component of a conical spin cycloid, polarization reversal by magnetic field was achieved [38]. Domain manipulation by dual magnetic and electric field control may provide a similar approach to exploit $\text{BiMn}_7\text{O}_{12}$'s ME coupling via inverse exchange striction and superposed ferrimagnetism.

In summary, we present an experimental realization and phenomenological model of ME coupling via inverse exchange striction in type I multiferroic $\text{BiMn}_7\text{O}_{12}$, which leads to a polar collinear magnetic structure uniquely stabilized in the presence of the electric polarization. Our findings represent a direct analog of related phenomena in type II multiferroics with $\uparrow\uparrow\downarrow\downarrow$ -based magnetic structures. Microscopically, we attribute the E -type AFM order to a modulation of superexchange pathways between Mn^{3+} B sites due to the stereochemical instability of Bi^{3+} ions. In contrast to the model type I multiferroic BiFeO_3 , $\text{BiMn}_7\text{O}_{12}$ hosts superposed orthogonal FIM modes supported by A - B exchange that may offer an avenue to multifunctionality via domain control.

- [1] N. A. Spaldin, S. W. Cheong, and R. Ramesh, *Phys. Today* **63** (10), 38 (2010).
- [2] N. A. Hill, *J. Phys. Chem. B* **104**, 6694 (2000).
- [3] S. Dong, J. M. Liu, S. W. Cheong, and Z. Ren, *Adv. Phys.* **64**, 519 (2015).
- [4] A. S. Borovik-Romanov, H. Grimmer, and M. Kenzelmann, Magnetic properties, in *International Tables for Crystallography, Volume D: Physical Properties of Crystals*, edited by A. Authier, 2nd ed. (Wiley, Hoboken, NJ, 2013), Chap. 1.5, pp. 106–153.
- [5] M. Kenzelmann, A. B. Harris, S. Jonas, C. Broholm, J. Schefer, S. B. Kim, C. L. Zhang, S. W. Cheong, O. P. Vajk, and J. W. Lynn, *Phys. Rev. Lett.* **95**, 087206 (2005).
- [6] T. Arima, A. Tokunaga, T. Goto, H. Kimura, Y. Noda, and Y. Tokura, *Phys. Rev. Lett.* **96**, 097202 (2006).
- [7] T. Kimura, *Annu. Rev. Mater. Res.* **37**, 387 (2007).
- [8] Y. J. Choi, H. T. Yi, S. Lee, Q. Huang, V. Kiryukhin, and S. W. Cheong, *Phys. Rev. Lett.* **100**, 047601 (2008).
- [9] J. van den Brink and D. I. Khomskii, *J. Phys.: Condens. Matter* **20**, 434217 (2008).
- [10] N. Furukawa and M. Mochizuki, *J. Phys. Soc. Jpn.* **79**, 033708 (2010).
- [11] M. Mochizuki, N. Furukawa, and N. Nagaosa, *Phys. Rev. Lett.* **105**, 037205 (2010).
- [12] R. D. Johnson and P. G. Radaelli, *Annu. Rev. Mater. Res.* **44**, 269 (2014).
- [13] Y. S. Chai, Y. S. Oh, L. J. Wang, N. Manivannan, S. M. Feng, Y. S. Yang, L. Q. Yan, C. Q. Jin, and K. H. Kim, *Phys. Rev. B* **85**, 184406 (2012).
- [14] S. Picozzi, K. Yamauchi, G. Bihlmayer, and S. Blügel, *Phys. Rev. B* **74**, 094402 (2006).
- [15] D. Khomskii, *Physics* **2**, 20 (2009).
- [16] S. Artyukhin, K. T. Delaney, N. A. Spaldin, and M. Mostovoy, *Nat. Mater.* **13**, 42 (2014).
- [17] Y. Kumagai and N. A. Spaldin, *Nat. Commun.* **4**, 1540 (2013).
- [18] I. Sosnowska and A. K. Zvezdin, *J. Magn. Magn. Mater.* **140-144**, 167 (1995).
- [19] C. Ederer and N. A. Spaldin, *Phys. Rev. B* **71**, 060401(R) (2005).
- [20] R. Przeniosło, M. Regulski, and I. Sosnowska, *J. Phys. Soc. Jpn.* **75**, 084718 (2006).
- [21] D. Lebeugle, D. Colson, A. Forget, M. Viret, A. M. Bataille, and A. Gukasov, *Phys. Rev. Lett.* **100**, 227602 (2008).
- [22] R. D. Johnson, P. A. McClarty, D. D. Khalyavin, P. Manuel, P. Svedlindh, and C. S. Knee, *Phys. Rev. B* **95**, 054420 (2017).
- [23] D. D. Khalyavin, A. N. Salak, N. M. Olekhnovich, A. V. Pushkarev, Y. V. Radyush, P. Manuel, I. P. Raevski, M. L. Zheludkevich, and M. G. S. Ferreira, *Phys. Rev. B* **89**, 174414 (2014).
- [24] C. D. Dashwood, L. S. I. Veiga, Q. Faure, J. G. Vale, D. G. Porter, S. P. Collins, P. Manuel, D. D. Khalyavin, F. Orlandi, R. S. Perry, R. D. Johnson, and D. F. McMorrow, *Phys. Rev. B* **102**, 180410 (2020).
- [25] A. A. Belik, Y. Matsushita, Y. Kumagai, Y. Katsuya, M. Tanaka, S. Y. Stefanovich, B. I. Lazoryak, F. Oba, and K. Yamaura, *Inorg. Chem.* **56**, 12272 (2017).
- [26] L. C. Chapon, P. Manuel, P. G. Radaelli, C. Benson, L. Perrott, S. Ansell, N. J. Rhodes, D. Raspino, D. Duxbury, E. Spill, and J. Norris, *Neutron News* **22**, 22 (2011).
- [27] J. Rodríguez-Carvajal, *Phys. B: Condens. Matter* **192**, 55 (1993).
- [28] H. T. Stokes, D. M. Hatch, and B. J. Campbell, ISOTROPY software suite, iso.byu.edu.
- [29] B. J. Campbell, H. T. Stokes, D. E. Tanner, and D. M. Hatch, *J. Appl. Crystallogr.* **39**, 607 (2006).
- [30] F. Mezzadri, G. Calestani, M. Calicchio, E. Gilioli, F. Bolzoni, R. Cabassi, M. Marezio, and A. Migliori, *Phys. Rev. B* **79**, 100106(R) (2009).
- [31] W. A. Sławiński, H. Okamoto, and H. Fjellväg, *Acta Crystallogr., Sect. B* **73**, 313 (2017).
- [32] See Supplemental Material at <http://link.aps.org/supplemental/10.1103/PhysRevB.107.L140402> for details of the crystal and magnetic structure refinements, mode decompositions, and transformation properties.
- [33] A. Gauzzi, G. Rousse, F. Mezzadri, G. L. Calestani, G. André, F. Bourée, M. Calicchio, E. Gilioli, R. Cabassi, F. Bolzoni, A. Prodi, P. Bordet, and M. Marezio, *J. Appl. Phys.* **113**, 043920 (2013).
- [34] F. Mezzadri, M. Buzzi, C. Pernechele, G. Calestani, M. Solzi, A. Migliori, and E. Gilioli, *Chem. Mater.* **23**, 3628 (2011).
- [35] In previous studies, the propagation vector was identified as $\mathbf{k} = (\frac{1}{2}, 0, \frac{1}{2})$ (*M* point of the Brillouin zone) which is distinct from the true propagation vector of $\mathbf{k} = (\frac{1}{2}, 0, -\frac{1}{2})$ at the *A* point.
- [36] N. Imamura, M. Karppinen, T. Motohashi, D. Fu, M. Itoh, and H. Yamauchi, *J. Am. Chem. Soc.* **130**, 14948 (2008).
- [37] R. D. Johnson, D. D. Khalyavin, P. Manuel, L. Zhang, K. Yamaura, and A. A. Belik, *Phys. Rev. B* **98**, 104423 (2018).
- [38] Y. Yamasaki, S. Miyasaka, Y. Kaneko, J. P. He, T. Arima, and Y. Tokura, *Phys. Rev. Lett.* **96**, 207204 (2006).